EFFECT OF VORTEX DEFLECTION ON VORTEX-ROTOR INTERACTION

Berend G. van der Wall, berend.vanderwall@dlr.de, DLR (Germany)

Abstract
Vortex-rotor interaction has been studied mostly with “rigid” straight-line vortices (longitudinal, lateral and orthogonal to the rotor disk). Vortex deformation during encounter with the rotor was only addressed by means of CFD codes. This paper investigates the interaction by a simplified vortex deflection model, where the interacting vortex is convected in parallel to the wake tube of the rotor once it penetrates the rotor disk. The consequences on rotor controls required to keep the trim constant are compared to former results obtained with a rigid (undeflected) vortex model.

1. INTRODUCTION

A limited number of investigations concerning the effects of rotorcraft encountering the tip vortex wake of fixed-wing aircraft have been conducted in the past decades and a comprehensive overview is given in [1]. The focus was on flight mechanics reaction and handling qualities of helicopters encountering a wake vortex by means of flight tests [2], comprehensive code simulation [3], and by use of ground-based simulators [4].

In all simulations the vortex was modelled as “rigid” and no mutual interaction with the helicopter and/or its downwash was considered. This was taken into account for the first time by means of CFD computations [5], with the observation that the vortex was immersed into the rotor wake and convected with it, which resulted in weaker rotor response, compared to that of a “rigid” vortex. Fig. 1 shows an example for slow forward flight with large rotor impact on the vortex and a high speed encounter with very little impact on vortex morphology.

This triggered investigations of the author first regarding the wake vortex hazard for rotorcraft encountering wind turbine wakes, because the number of wind energy power plants on the country side in Germany is huge and in notable proximity to airfields [6]. The downstream wake of such horizontal axis wind turbines is characterized by a spiral helix of usually three blade tip vortices on the surface of the wake tube.

This is justified because the number of blades is three for the overwhelming majority of the installed systems. When crossing the wake tube at its upper or lower boundary, i.e., in the immediate vicinity to the center of these vortices, the strong rotational swirl field of them acts on the interacting helicopter rotor blades, generating a change in rotor thrust, hub pitching and rolling moments, torque and hence power, flapping motion, etc. Recent investigations of the author made use of equivalent “rigid” vortices to investigate these effects, because this allows an analytical solution using blade element momentum theory [7].

In this paper, a simplified vortex deformation model based on momentum theory is used to quantify the amount of mitigation in dependence of flight speed (advance ratio μ). The basic assumption here is that the rotor wake tube is skewed by the mean induced velocity, and thus is a function of rotor thrust coefficient C_T, advance ratio, rotor angle of attack (= disk tilt angle) α, and the total rotor inflow ratio $\lambda = \lambda_i + \mu_z$.

The principle is sketched in Fig. 2. Therein, the red solid line represents a “rigid” vortex as used in former studies, the wake tube for two advance ratios of $\mu = 0.05$ and 0.3 is indicated by thin black lines, and once the interacting vortex penetrates the rotor disk it will be convected downstream with the rotor wake, sketched by the dashed red line. As suggested by the figure, a small advance ratio will lead to large deviation from the “rigid” vortex trajectory, and with increasing advance ratio this deviation progressively diminishes, such that at an advance ratio from $\mu = 0.2$ on the deviation from the “rigid” vortex becomes very small.

Obviously, this is a nonlinear effect, because the reduction of the mean induced velocity with advance ratio is highly nonlinear and asymptotically approaches zero for $\mu \to \infty$. Therefore, the impact of a vortex deformation will be largest at low μ, and smallest for large μ.

Presented at 45th European Rotorcraft Forum, Warsaw, Poland, 17-20 September, 2019

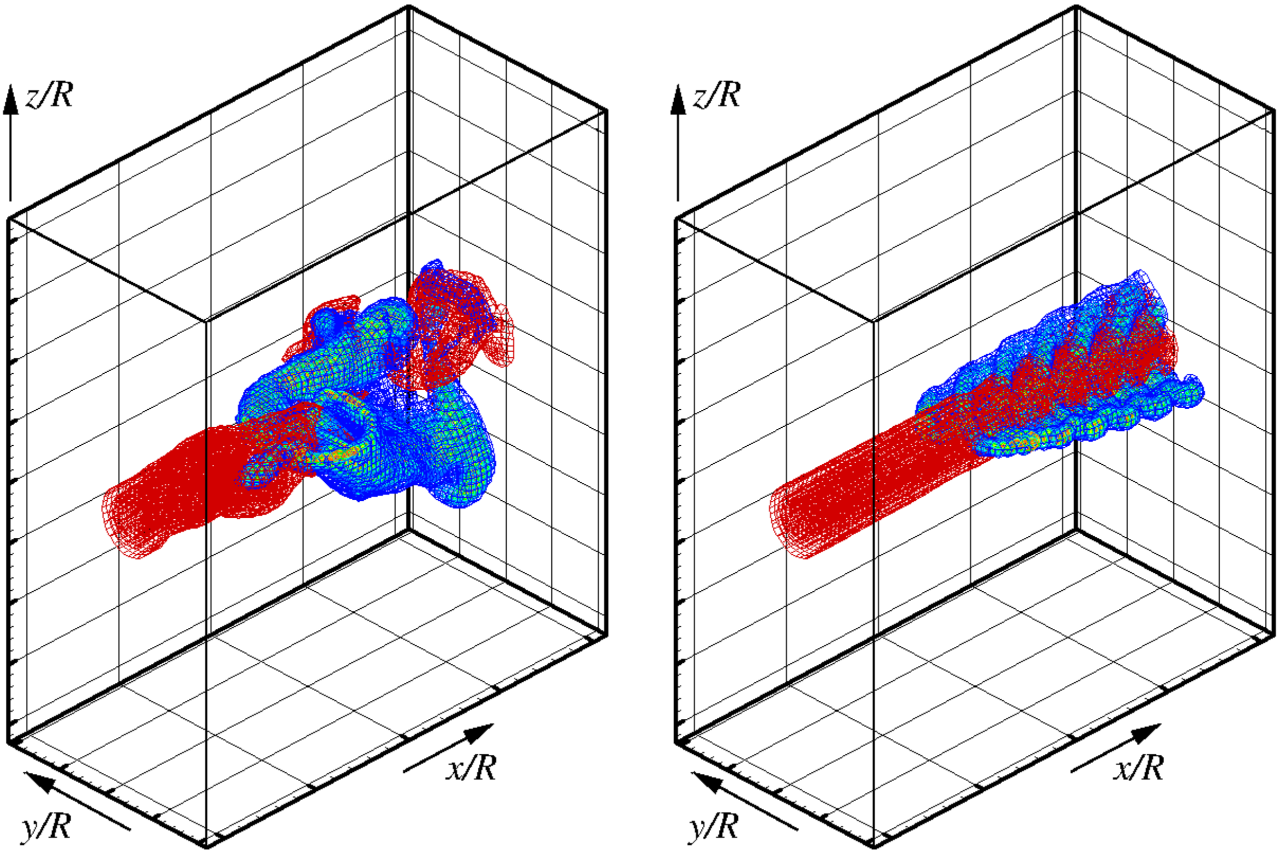

(a) Small advance ratio, $\mu = 0.05$ (b) Large advance ratio, $\mu = 0.35$

Fig. 1. Vortex and rotor wake morphology during a parallel interaction, from [5].

2. MODELLING OF THE VORTEX DEFORMATION

The interacting vortex is a semi-infinite straight-line vortex until its impingement on the rotor disk, see Fig. 2. From that point on it is continued as a second semi-infinite long straight-line vortex, but inclined by the wake skew angle.

This assumption is justified, because the vortex consists of air, as does the air inside the wake tube, which is generated by the rotor thrust and its induced velocities. Momentum theory in forward flight leads to a quartic to solve for the induced inflow ratio λ_i and with it for the total inflow ratio, Eq. (1). Therein, μ_z is the inflow ratio normal to the disk due to flight speed V_∞ and disk tilt angle; μ accordingly is the inflow ratio in the plane of the disk. The rotor blade tip speed ΩR is used for nondimensionalization of all velocities. This equation requires an iterative solution until convergence is obtained. λ_h is the induced inflow ratio in hover, where $\mu = 0$.

(1) $$\lambda_i^4 + 2\mu_z\lambda_i^3 + \mu^2\lambda_i^2 - \lambda_h^4 = 0; \qquad \lambda_h = \sqrt{C_T/2}$$
$$\mu = V_\infty \cos\alpha/(\Omega R); \quad \mu_z = -\mu\tan\alpha$$

Next, the wake skew angle χ needs to be computed, based on the velocities acting in the plane of the rotor and normal to it, see Fig. 2.

(2) $$\chi = \arctan\frac{\mu}{\lambda_i + \mu_z}$$

As an example for the behavior of the mean induced inflow ratio with respect to advance ratio and roto thrust coefficient are given in Fig. 3 for zero rotor angle of attack, such that the argument of Eq. (2) reduces to μ/λ_i. Zero thrust generates zero induced inflow ratio, thus the wake skew angle then is 90 deg for all advance ratios. With increasing thrust the induced inflow ratio grows proportionally to the square root of the thrust coefficient, but asymptotically diminishes with advance ratio.

In consequence the wake skew angle is quickly approaching 90 deg. Typical thrust coefficients of helicopter rotors are about $C_T = 0.008$ and maximum advance ratios around 0.35, where it can be seen from Fig. 3 that the wake skew angle is close to 90 deg, and major vortex deflections will only occur for advance ratios less than 0.2.

Presented at 45th European Rotorcraft Forum, Warsaw, Poland, 17-20 September, 2019

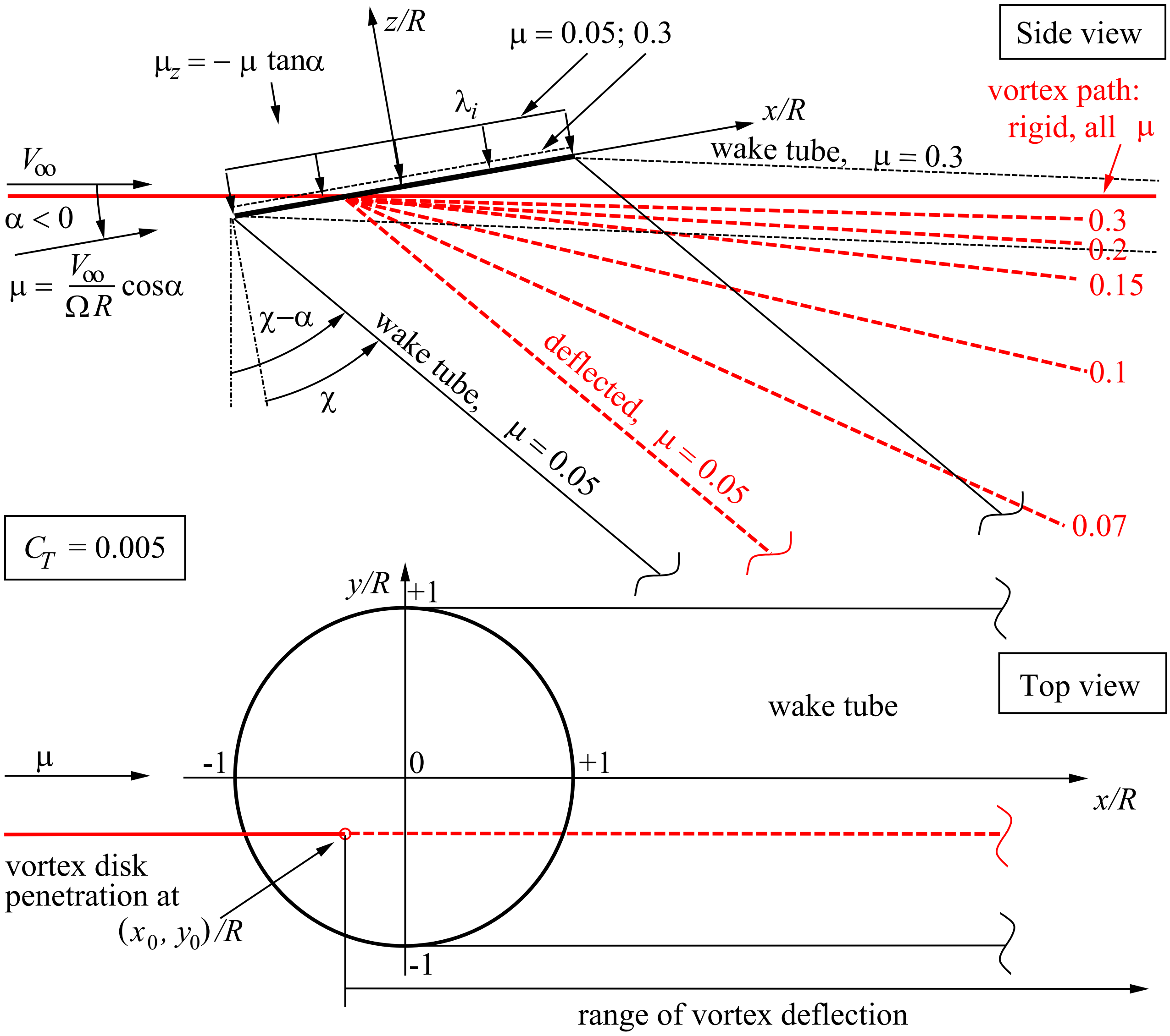

Fig. 2. Principle of the deflected vortex model.

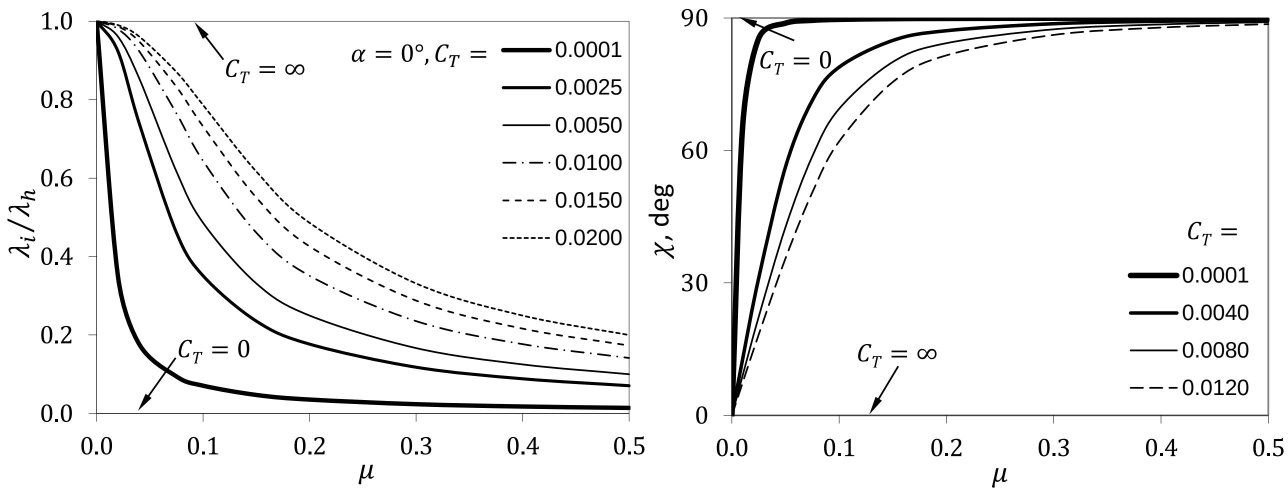

(a) Induced inflow ratio (b) Wake skew angle for $\alpha = 0°$

Fig. 3. Induced inflow ratio and resulting wake skew angle for zero rotor angle of attack.

Presented at 45th European Rotorcraft Forum, Warsaw, Poland, 17-20 September, 2019

3. ROTOR INVESTIGATED

The four-bladed Mach scaled Bo105 model rotor is used as example rotor with a radius of $R = 2$ m, a root cutout of 22% radius, a chord length of $c = 0.121$ m, has a rectangular blade planform leading to a solidity of $\sigma = 0.077$. The airfoil is a NACA23012 with a trailing edge tab, the blade has a linear twist of -8 deg per radius and it operates at a rotational frequency of $\Omega = 109$ rad/s resulting in a tip speed of $\Omega R = 218$ m/s. Elastic rotor blades are modeled using two flapping modes and one lead-lag and one torsion mode. The induced downwash model of Mangler and Squire is employed and unsteady blade element aerodynamics are used. 40 blade elements represent a sufficiently high resolution along the blade radial axis, Fig. 4, and 2 deg azimuth steps are used for time integration.

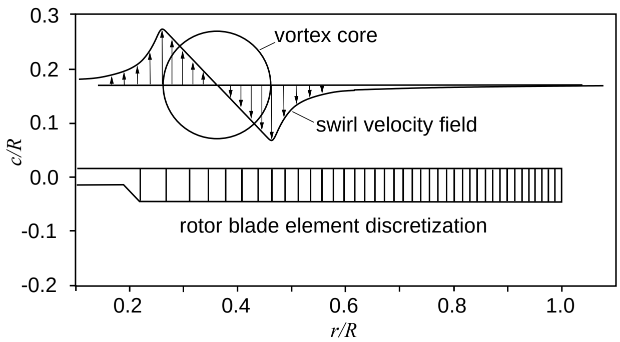

Fig. 4. Bo105 rotor blade discretization.

As in former publications of the author a nondimensional strength of $\lambda_{V0} = \Gamma/(2\pi\Omega R^2) = 0.01$ and a core radius of $r_c = R_c/R = 0.1$ are chosen for the interacting vortex. The vortex core diameter thus extends more than three chord lengths and covers a minimum of 8 blade elements when oriented normal to the blade axis as shown in Fig. 4. During a parallel interaction with the blade, the blade tip passes a length of $0.0349R$ and thus experiences almost 6 steps inside the vortex core radius; all inner radial positions experience more (up to 26 steps for the root cutout) time steps inside the vortex core. Therefore, vortex orientations normal and parallel to the blade axis are sufficiently well resolved both in space and in time.

The rotor is trimmed in undisturbed atmosphere with a constant flat plate drag area virtually representing the fuselage drag that needs to be compensated by tilting the rotor forward to generate an equal amount of propulsive force. The rotor is trimmed to zero hub moments and a constant thrust of 3750 N (equivalent to a 2.3 t Bo105 helicopter) which represents a thrust coefficient of $C_T = 0.005126$, resulting in a specific blade loading of $C_T/\sigma = 0.0666$. The degrees of freedom to obtain the trim goal are the shaft angle of attack α, the collective control angle θ_0, the longitudinal control angle Θ_S and the lateral control angle Θ_C. Since the dynamic pressure is increasing to the square of the flight speed the shaft angle will represent this behavior as is illustrated in Fig. 5.

Following momentum theory the mean induced velocity is largest in hover and quickly reduces with increasing flight speed as also shown in Fig. 5. However, the total normal rotor inflow is increasing with flight speed due to forward tilt of the rotor disk. Therefore, a high total inflow exist in hover (dominated by induced velocity) and high speed flight (dominated by inflow due to disk tilt), and less inflow at moderate speeds. Consequently, the collective control angle needed to generate thrust is large in hover and high speed, and less at moderate speed. It is, however, also depending on the longitudinal control angle that is needed to compensate the asymmetry of dynamic pressure on the advancing and retreating side of the rotor, which increases to the square of the flight speed. Therefore, the longitudinal control angle represents this square curve behavior. In hover, with rotational symmetry of flow conditions, the cyclic controls are all zero.

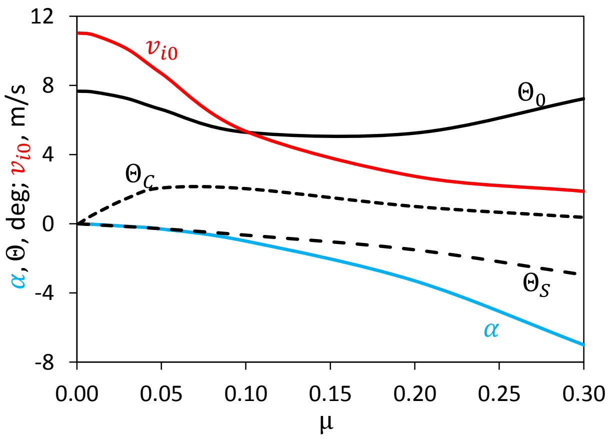

Fig. 5. Rotor trim in undisturbed air.

Finally the lateral control angle rises during the transition from hover to moderate speeds and slowly decays with increasing flight speed thereafter. This is driven by the longitudinal gradient in the induced velocities generated by the Mangler/Squire model applied here. The gradient is zero in hover, thus zero cyclic control angle, largest during transition where the mean induced velocity still is large, an decays in parallel to the diminishing mean induced velocities.

Next, the power required by the rotor P is shown in Fig. 6. It mainly depends on the product of total inflow and thrust, therefore it is quite similar in shape to the collective control angle for the same reasons. In high speed flight compressibility effects on the advancing side and stall impact on the retreating side may further increase airfoil power, but the maximum advance ratio here is $\mu = 0.3$ where these is-

Presented at 45th European Rotorcraft Forum, Warsaw, Poland, 17-20 September, 2019

sues only play a minor role. The wake skew angle in the geodetic system $\chi - \alpha$ and in the rotor shaft axis system χ are given in Fig. 6 as well. In hover the wake is vertically blown downwards, thus $\chi = \chi - \alpha = 0°$ because $\alpha = 0°$. In high speed flight $\chi - \alpha$ asymptotically approaches 90° because the induced velocity asymptotically approaches zero. In the shaft axis system, however, the increasing nose-down tilt of the disk is affecting the more and more the angle relative to the disk. In the extreme, when the rotor is tilted forward by -90° (= propeller) against the flight direction, the skew angle in the shaft system will be again $\chi = 0°$.

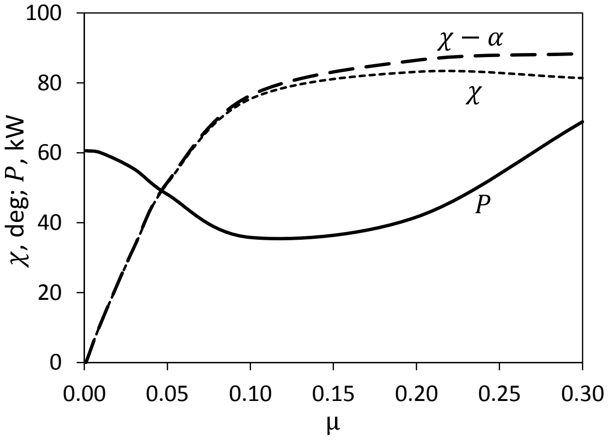

Fig. 6. Power required and wake skew angle.

Further results shown in Fig. 7 are the steady and 1/rev components of the first flapping, lagging and torsion modes at the blade tip. The steady flapping β_0 is the elastic deformation relative to the built-in precone angle. It is almost constant for the range of advance ratios due to constant thrust, slight shifts of the radial center of blade lift cause equally slight variations of steady coning.

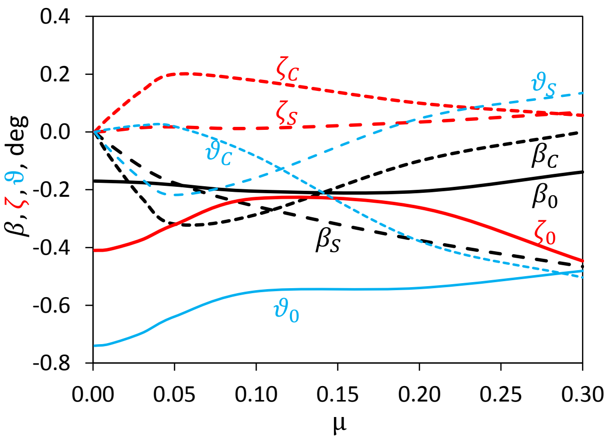

Fig. 7. Steady and 1/rev components of the first flapping, lagging and torsion modes.

Steady lag ζ_0 represents the power curve; positive deflection is in rotational direction, thus all steady lag is backwards due to induced drag and due to airfoil drag acting against the rotation. The steady torsion ϑ_0 in average is around -0.6 deg mainly due to the propeller moment.

Due to zero hub moment trim the cyclic blade flapping remains at rather small values, as does the cyclic lagging and torsion, but the latter is increasing in magnitude with increasing advance ratio because stronger aerodynamic moments act at the blade tip especially on the advancing side.

All following results that include a vortex either as rigid or deflected by the rotor downwash are including a retrim of the rotor. The difference to the trim results in undisturbed air are shown and explained.

4. RESULTS

First, the baseline case in undisturbed air without a vortex was trimmed (results see previous section); second, a trim with a rigid vortex followed (as done in prior publications); and third, a trim with vortex deformation as sketched in Fig. 2 was performed. The difference in trim controls with respect to the baseline (= undisturbed air) trim is related to the nondimensional vortex strength as done in prior publications, showing the differences between the impact of a rigid and a deformed vortex.

The vortex passes the rotor disk in its center and its lateral position is varied along the rotor y axis from two rotor radii left of it to the same amount right of it. Therefore, in the front of the rotor disk the vortex position relative to it is the same for the rigid and the deformed vortex, but in the rear half of the disk the vortex deformation becomes effective. At every lateral position of the vortex a trim is performed. Black lines represent the influence of a "rigid" vortex, red lines those of a deformed vortex as sketched in Fig. 2.

4.1. Wake skew angle

To better understand the following results, the geometries of both the rigid and the deflected vortex are shown in Fig. 8 for different advance ratios. The wake skew angles can be taken from Fig. 6. In Fig. 8 (a) for a very small advance ratio of $\mu = 0.01$ the rotor downwash is dominating and strongly deflects the oncoming vortices from the point of its penetration of the rotor disk. Compared to the rigid vortex in black the deflected vortices show a large change of orientation.

Depending on their longitudinal position of the penetration point the deflected vortices will have a rather small influence on the rotor blade aerodynamics when this point is at the front end of the disk $x_0/R = -1$ (solid blue line). They at least will have a

Presented at 45th European Rotorcraft Forum, Warsaw, Poland, 17-20 September, 2019

strong impact on the front half of the rotor disk but not in the rear when penetrating the disk in the rotor center ($x_0/R = 0$, red line) and they will have a quite similar impact when penetrating the disk at the rear end ($x_0/R = +1$, dashed blue line).

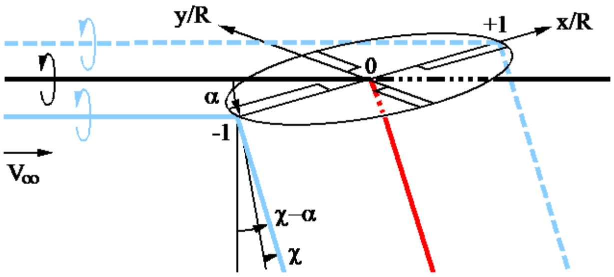

(a) Small advance ratio $\mu = 0.01$

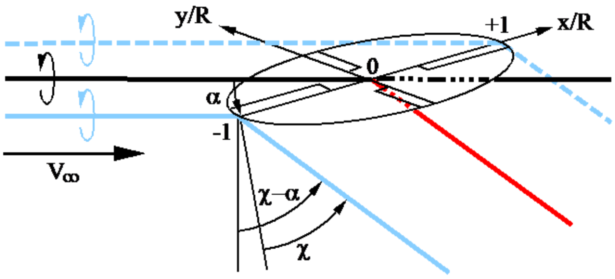

(b) Low to moderate advance ratio $\mu = 0.05$

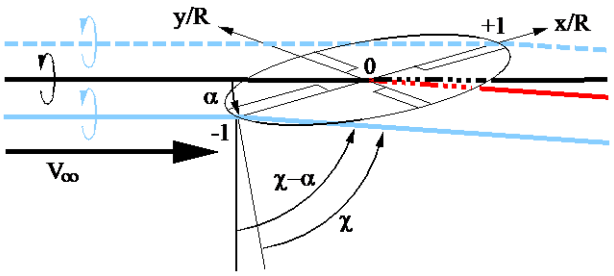

(c) High advance ratio $\mu = 0.3$
Fig. 8. Geometry of rigid and deflected vortices for different advance ratios.

Because the wake skew angle χ quickly increases already during the transition phase from hover with $\chi = 0$ deg to forward flight, see Fig. 6, advance ratios even as low as $\mu = 0.05$ will have already have $\chi = 51$ deg. This leads to a much less vortex deflection from the horizontal plane as sketched in Fig. 8 (b) compared to Fig. 8 (a), positioning the vortices closer to the disk.

At high advance ratios the wake is almost parallel to the flight direction with only little deflection relative to it, Fig. 8 (c). Thus it can be assumed with reasonable justification that at this high advance ratio the differences between results using a rigid vortex and those using a deflected vortex will be almost identical, because the vortex position relative to the rotor disk is only marginally affected.

4.2. Control angles required to retrim the rotor

Two examples for the influence of advance ratio on rotor controls required for retrim are given in Fig. 9 (a) and (b) representing the conditions of Fig. 8 (b) and (c). The vortex sense of rotation is always clockwise looking upstream. It can be seen that at high advance ratio, Fig. 9 (b), there is virtually no difference between the rigid vortex and the deflected vortex as would have been suggested by the little amount of deformation sketched in Fig. 2 and Fig. 8 (c). At small advance ratio the deviation is much larger, Fig. 9 (a), and especially the collective and longitudinal cyclic control angles are smaller than for the "rigid" vortex interaction, confirming the CFD results of [5].

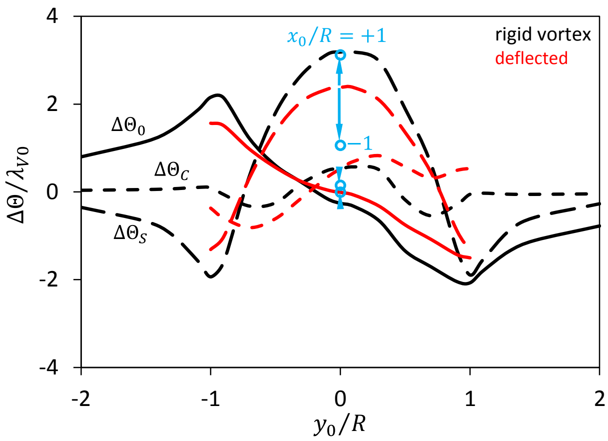

(a) $\mu = 0.05$

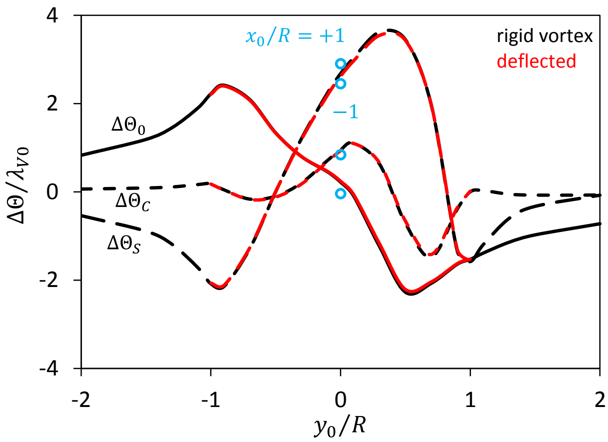

(b) $\mu = 0.3$
Fig. 9. Rotor controls required to maintain trim.
Lines: vortex at $x_0/R = 0$; blue circles: $x_0/R = \pm 1$

The lines in Fig. 9 are for a vortex penetrating the rotor disk at its center in longitudinal direction, i.e. at $x_0/R = 0$. A further reduction must be expected when the penetration point moves to the front end of the rotor disk, i.e. at $x_0/R = -1$, and this case is additionally shown in Fig. 9 (a) by blue circles; the blue arrows indicate the further reduction of controls required. A penetration of the rotor disk at its rear end,

Presented at 45th European Rotorcraft Forum, Warsaw, Poland, 17-20 September, 2019

$x_0/R = +1$, also represented by a blue circle in Fig. 9 (a), leads to a result practically the same as obtained using the rigid vortex. This was expected because now the vortex affects the entire disk practically the same as the rigid vortex, only at the rear gets the deflection downwards, but this does affect the rotor only marginally.

At high advance ratio, Fig. 9 (b), the vortex penetration point has much less effect, because the vortex deflection is much less and its position relative to the rotor disk is only little modified, even for penetration points at the front end of the disk.

The physics behind the shape of the curve have been outlined in [7] and are repeated here at the example of Fig. 9 (a). Vortex positions far away from the rotor to either side have a vanishing influence due to vanishing induced velocities at the rotor. A position at the left side $y_0/R = -1$ induces the maximum average normal velocity oriented downwards (the sense of rotation was defined as clockwise seen upstream), thus requiring a positive collective to come up for the loss. Also, the lateral gradient of velocities is maximum at this position, requiring a negative longitudinal control to come up for the loss of lift on the retreating side.

A vortex position at the right side $y_0/R = +1$ induces the maximum average normal velocity oriented upwards (the sense of rotation was defined as clockwise seen upstream), thus requiring a negative collective to come up for the loss. Again, the lateral gradient of velocities is maximum at this position, requiring a negative longitudinal control to come up for the loss of lift on the retreating side.

Finally, a vortex position in the rotor center induces as much downwash on the advancing side as upwash on the retreating side, such that the overall thrust remains unaffected and no collective control is needed. However, an opposite induced velocity gradient across the disk is present now, hence the longitudinal control to eliminate the associated aerodynamic rolling moment is positive.

An increasing advance ratio introduces some asymmetry due to increasing dynamic pressure on the advancing side and a reduction of it on the retreating side. This also couples the collective and longitudinal cyclic control angles, because any collective control modifies primarily the thrust but also the aerodynamic rolling moment, as does any longitudinal cyclic control primarily affects the aerodynamic rolling moment, but also the thrust.

4.3. Influence of the vortex deflection

A comparison of the results obtained using a rigid vortex (black lines) and a vortex that is deflected from the point of penetration of the rotor disk (red lines) is given in Fig. 10 (a) for the collective control angle, in (b) for the longitudinal cyclic control angle and in (c) for the rotor power. The line style denotes different advance ratios from close to hover to $\mu = 0.3$.

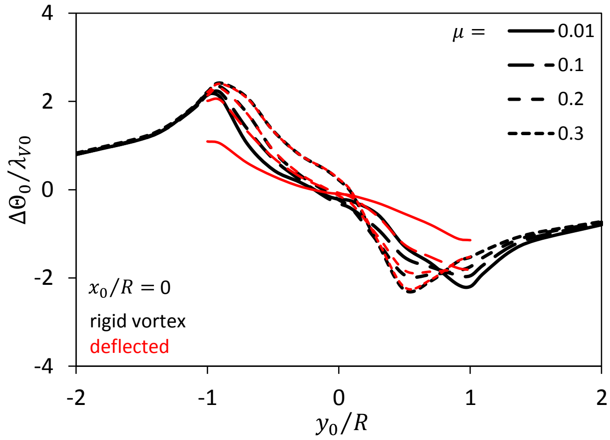

(a) Collective control angle

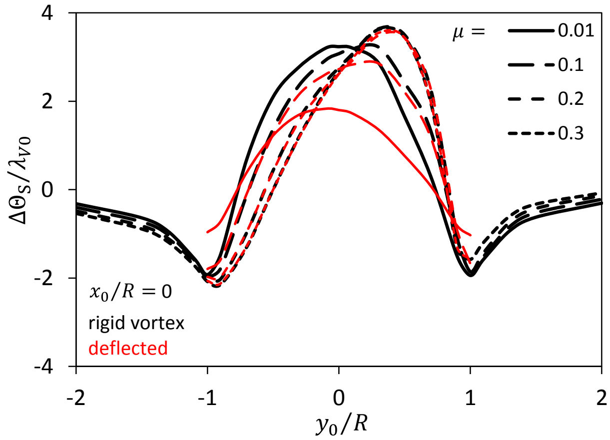

(b) Longitudinal control angle

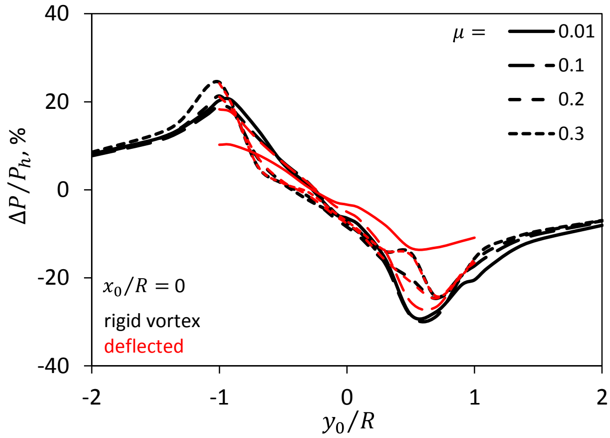

(c) Rotor power

Fig. 10. Vortex effect on rotor controls and power.

In any of the figures the effect of vortex deflection is largest near hover, where the vortex from the point

Presented at 45th European Rotorcraft Forum, Warsaw, Poland, 17-20 September, 2019

of disk penetration on is almost vertically deflected, mainly inducing in-plane velocities with the deflected part of it, see Fig. 8 (a). Only the undeflected part lies in the plane of the rotor from the front end to its center, inducing normal velocities only in the front half of the disk, in contrast to a rigid vortex that affects the entire disk. Therefore, controls required to retrim and the impact on change of power is only about half of the values obtained with a rigid vortex (solid lines).

At an advance ratio of $\mu = 0.1$ (long dashed lines) the vortex deflection is much less, see Fig. 2, and the deflected part of the vortex will still have a significant impact on the rear half of the disk, although not as much as the rigid vortex. Consequently the results obtained with a deflected vortex are much closer to the rigid vortex results as near hover, Fig. 10. For advance ratios of $\mu \geq 0.2$ the vortex deflection is very small, see Fig. 2 and Fig. 8 (c), and the results shown in Fig. 10 are almost undistinguishable from those using a rigid vortex assumption. Therefore, from advance ratios beginning at about $\mu = 0.2$ on the rigid vortex assumption may be used with good accuracy.

The physics behind the shape of the power curve have been outlined in [8] and are repeated here at the example of Fig. 10 (c). Vortex positions far away from the rotor to either side have a vanishing influence due to vanishing induced velocities at the rotor. A position near the left side $y_0/R = -1$ induces the maximum average normal velocity oriented downwards (the sense of rotation was defined as clockwise seen upstream), thus adding inflow to the rotor (similar to a climb condition) which causes an increase in induced power.

The opposite happens for vortex positions near the right side $y_0/R = +1$, where the vortex-induced velocities partly reduce the thrust-induced inflow (similar to a descent condition), which reduced the induced power.

Vortex positions near the rotor center increase the inflow on the advancing (right) side, reducing it on the opposite (left) side, which in total has a neutral effect on power. With increasing advance ratio the power curve does not change significantly except for a larger power loos for vortex positions on the advancing side than the power increase for vortex positions on the retreating side.

Aside from the vortex influence on rotor control angles and power required its impact on modification of mean and cyclic blade flapping is of interest, and on the rotor control ratio (RCR). This is defined as the sum of collective and cyclic controls needed, divided by the amount of available control angle remaining from the trim to the hard stops of the control mechanism. Although the latter depends on the advance ratio and the available margin will shrink with increasing advance ratio (see Fig. 5: at high μ both the collective and the cyclic control angles grow quickly), here for simplicity the margin is assumed to be constant at an amount of 8°.

Steady elastic flapping mostly is associated with the rotor thrust, which is held constant throughout all variations. However, the radial center of blade lift may vary with the vortex influence, and this is shown in Fig. 11 (a). The effect is small compared to the amount of control angle required to retrim (see Fig. 10 (a)), but it is systematic. Vortex positions at half of the radius right or left of the rotor center have the maximum influence on shifting the center of lift, because then the outer half of the blade at the respective right or left positions experience an upwash and the inner part a downwash, or vice versa on the opposite side of the rotor.

The longitudinal flapping response shown in Fig. 11 (b) is mainly responding to lateral asymmetries in blade lift as caused by vortex positions on the right or left end of the disk, and an opposite gradient for a central position, for the same reasons as outlined before at the example of the longitudinal control angle, see Fig. 10 (b) for comparison. Again, the retrim to zero hub moments eliminates the major part of the vortex influence and the remaining elastic response in 1/rev is small compared to the cyclic control required to retrim.

Finally, the RCR is given in Fig. 11 (c), merging the collective and cyclic control required for retrim (shown before in Fig. 10 (a) and (b)) and relating the result to the available control margin. In this example the smallest RCR values are obtained near hover (solid lines) with the RCR of vortex deflection (red) only about half the value of a rigid vortex (black). With increasing advance ratio the advancing side positions of the vortex become more severe than the retreating side positions. Also, from $\mu = 0.2$ on the RCR of rigid and deflected vortex are practically the same, which is due to very small deflection angles.

4.4. Influence of the advance ratio

The difference between results of the rigid vortex assumption and the deflected vortex are best seen when plotting characteristic values versus the advance ratio, which is done in Fig. 12. Fig. 12 (a) shows the collective control angle at vortex positions at the left end of the rotor disk $y_0/R = -1$, where near hover the deflected vortex (red) has about half of the effect than the rigid vortex (black) as was shown in Fig. 10 (a). With increasing advance ratio the difference quickly reduces and from $\mu = 0.2$ on both curves are merging.

Presented at 45th European Rotorcraft Forum, Warsaw, Poland, 17-20 September, 2019

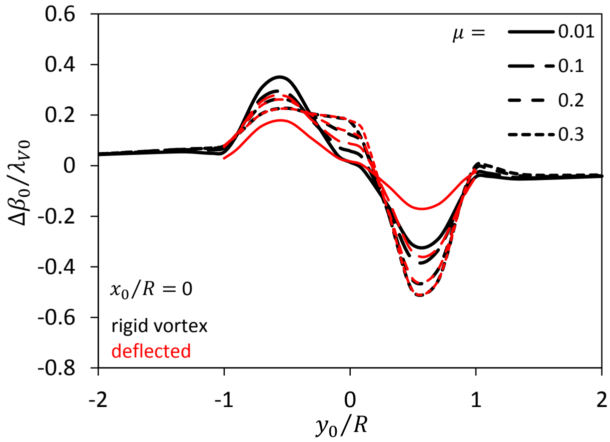

(a) Mean elastic flap deflection

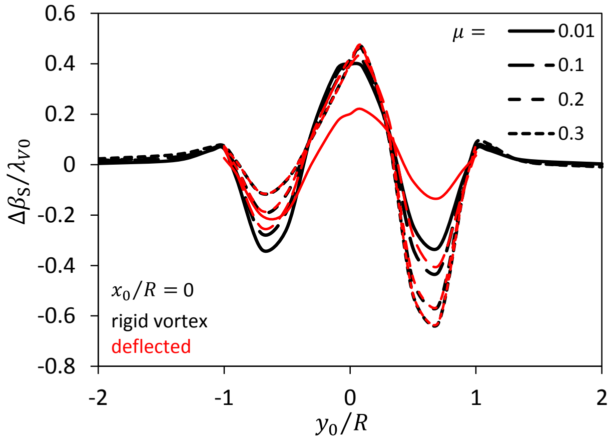

(b) Lateral elastic flapping

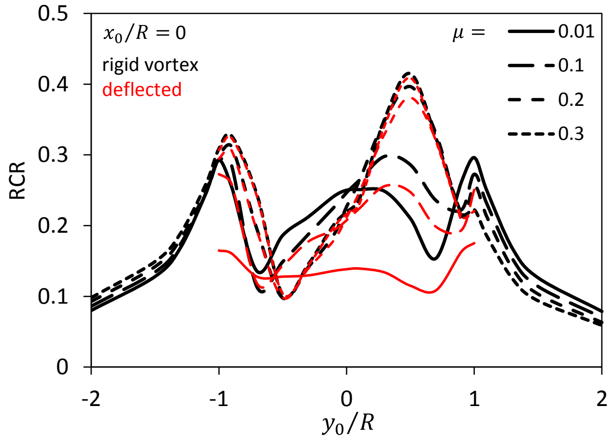

(c) Rotor control ratio

Fig. 11. Vortex effect on rotor blade flapping and on rotor control ratio.

In addition the maximum values are plotted that are obtained at slightly more inboard vortex positions than $y_0/R = -1$. Again, for $\mu \geq 0.2$ the rigid and deflected vortex lead to about the same results and the use of the rigid vortex model appears justified.

The mean elastic blade flapping variation is given in Fig. 12 (b) for vortex positions at $y_0/R = 0.5$, where in Fig. 11 (a) the maximum response was found. The general trend with advance ratio is an increasing downwards flapping. This indicates the center of blade lift for this vortex position moves more and more inboard, thus reducing the moment about the blade attachment while the opposing moment from centrifugal forces remains constant.

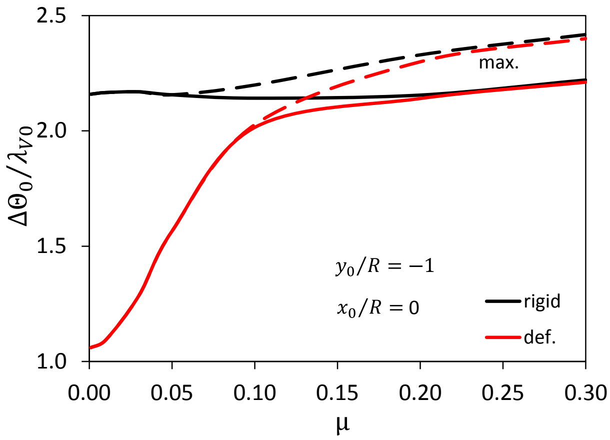

(a) Collective control angle

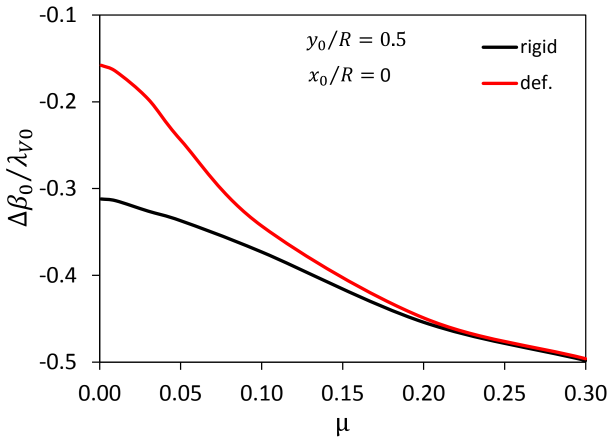

(b) Mean elastic flap deflection

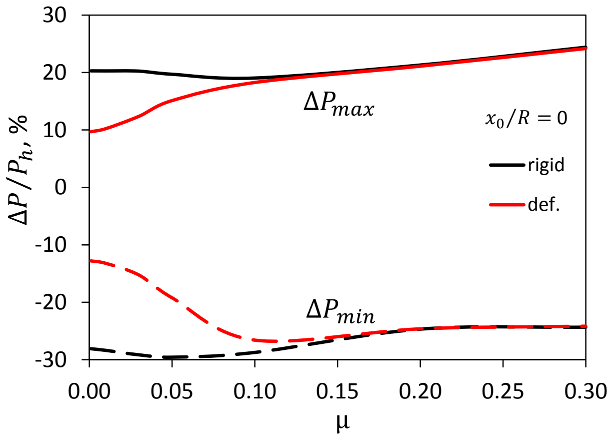

(c) Rotor power

Fig. 12. Vortex effect on collective control, mean elastic flapping and power.

Presented at 45th European Rotorcraft Forum, Warsaw, Poland, 17-20 September, 2019

As before the deflected vortex near hover has about half of the impact than the rigid vortex, but from $\mu = 0.2$ on both curves are merging. Finally, the rotor power maximum and minimum due to the vortex influence are shown in Fig. 12 (c). The overall trend is quite similar to the former observations.

Remaining parameters are the longitudinal control angle, the lateral flapping associated with it, and the RCR, all shown in Fig. 13 (a)-(c). In addition to the vortex penetration point in the rotor center at $x_0/R = 0$ a point in the front end at $x_0/R = -1$ (blue solid line) and at the rear end at $x_0/R = +1$ (blue dashed line) are added. The lateral vortex position is always the rotor center $y_0/R = 0$. However, as seen in Fig. 10 (b) the maximum vortex influence shifts to different lateral positions with increasing advance ratio from $\mu = 0.1$ on; therefore it is also given in the graphs as black dashed curve only for the rigid vortex computations and denoted as "rigid, max.". This can be significantly larger than the influence at $y_0/R = 0$.

As expected the vortex front position, where it is deflected right at the beginning of the rotor disk, has only very little impact on the rotor control, flapping and RCR, while the deflection at the rear end of the rotor has an impact very close to that of the rigid vortex. Because at high advance ratios the deflection is becoming increasingly smaller all curves are getting close together for $\mu \geq 0.2$.

In hover, the longitudinal control angle requires a large inputs to compensate a rigid vortex influence on trim, because it crosses the entire rotor disk, Fig. 13 (a), solid black line. A vortex deflected downward at the front end of the disk (solid blue line) leaves the entire disk almost unaffected, thus very little control is needed for retrim. When the vortex penetrates the center of the disk and then is deflected downwards it covers the entire front, but not the rear half of the disk and about half of the rigid vortex magnitude is required in the control angle (solid red line). Finally, when the vortex penetrates the disk at tits rear end, the entire disk is affected and the control required is very close to that of the rigid vortex (dashed blue line).

With increasing advance ratio all curves get close together because the vortex deflection angles quickly diminish with increasing speed of flight. However, it is observed already from Fig. 10 (b) that the maximum of control required is shifting to vortex positions more on the advancing side than in the middle of the disk. Therefore, these maximum values are obtained from the rigid vortex computations only and added to the figure for comparison (dashed black line). It indicates that with increasing advance ratio the maximum control required is increasing as well.

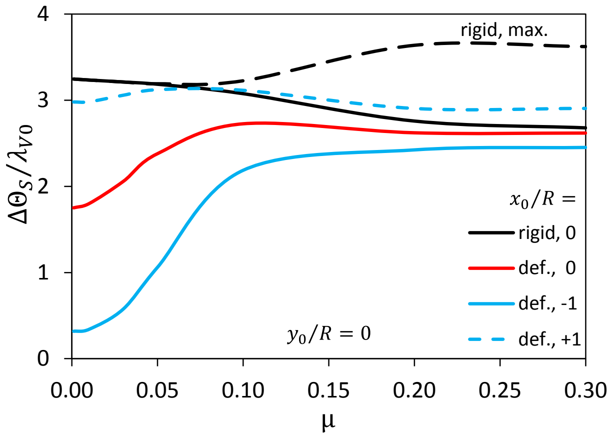

(a) Longitudinal control angle

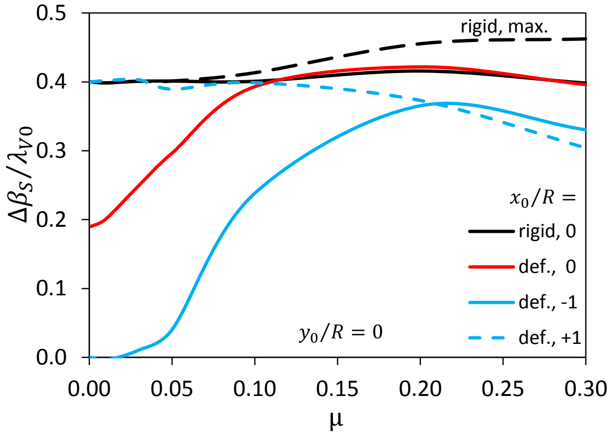

(b) Lateral flapping

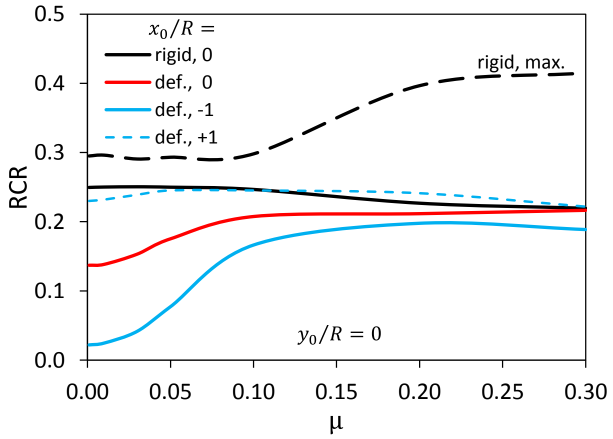

(c) Rotor control ratio

Fig. 13. Vortex effect on longitudinal control angle, lateral flapping and rotor control ratio.

The longitudinal flapping reaction is given in Fig. 13 (b) in the same manner and the overall behavior is quite similar to the one observed in the longitudinal control angle. Because the RCR is dominated by the longitudinal control angle deflections given in Fig. 13 (a). The amount of collective for central vortex positions is close to zero, see Fig. 10 (a), the RCR curve forms are almost the same as for the

Presented at 45th European Rotorcraft Forum, Warsaw, Poland, 17-20 September, 2019

longitudinal control angle.

The RCR given in Fig. 13 (c) at all instances is always less than 0.5, which means more than half of the available control margin is still left unused, and thus considered nonhazardous. A value of 1 means that all available margin is consumed for retrimming and values exceeding 1 indicate the disturbance cannot be fully counteracted by the pilot.

5. CONCLUSIONS

In this paper the impact of a vortex interacting with a rotor is investigated for a straight “rigid” vortex and a vortex that is deflected following the rotor downwash tube when penetrating the rotor disk, thus changing its orientation to it. The major findings are listed below.

- It is shown that the vortex deflection due to the rotor downwash is nonlinearly depending on the advance ratio.
- For small advance ratio the vortex deflection is largest, and the impact on rotor response can largely be reduced relative to a “rigid” undeflected vortex.
- At large advance ratios, however, the vortex deflection is small and only a minor reduction of the rotor response is observed.
- Therefore, former results with “rigid” vortex-rotor interaction are confirmed in their magnitude at high advance ratios for $\mu \geq 0.2$, where the rotor response was largest, while at small advance ratio the vortex is “blown away” by the rotor’s induced velocity, thus reducing its impact.

6. REFERENCES

[1] van der Wall, B.G., Lehmann, P.H., “About the impact of wind turbine blade tip vortices on helicopter rotor trim and rotor blade motion,” *CEAS Aeronautical Journal*, **9**(1): 67-84, 2018

[2] Mantay, W.R., Holbrook, G.T., Campbell, R.L. and Tamaine, R.L., “Helicopter response of an airplane’s trailing vortex,” *Journal of Aircraft*, **14**(4): 357-363, 1977

[3] Azuma, A., Saito, S., Kawachi, K.: “Response of a helicopter penetrating the tip vortices of a large airplane,” *VERTICA*, **11**(1): 65–76, 1987

[4] Turner, G. P., Padfield, G. D., and Harris, M., “Encounters with Aircraft Vortex Wakes; The Impact on Helicopter Handling Qualities,” *Journal of Aircraft*, **39**(5): 839–849, 2002

[5] Whitehouse, G.R., Brown, R.E.: Modelling a helicopter rotor’s response to wake encounters. *Aeronautical Journal*, **108**(1079): 15–26, 2004

[6] van der Wall, B.G., Fischenberg, D., Lehmann, P.H., van der Wall, L.B.: *Impact of Wind Energy Rotor Wakes on Fixed-Wing Aircraft and Helicopters,* 42nd European Rotorcraft Forum, Lille, France, Sept. 5–8, 2016.

[7] van der Wall, B.G., van der Wall, L.B., “Analytical Estimate of Rotor Controls Required for a Straight Vortex Disturbance Rejection,” *Journal of the American Helicopter Society*, **62**(1): 015001-1-4, 2017

[8] van der Wall, B.G.: *Rotor Thrust and Power Variations During In-Plane and Orthogonal Vortex Interaction*, 7th Asian/Australian Rotorcraft Forum, Seogwipo City, Jeju Island, Korea, Oct. 30 – Nov. 1, 2018

Presented at 45th European Rotorcraft Forum, Warsaw, Poland, 17-20 September, 2019